ELSEVIER

Materials Chemistry and Physics 78 (2002) 160–169

MATERIALS CHEMISTRY AND PHYSICS

www.elsevier.com/locate/matchemphys

Emission spectra of $LnPO_4:RE^{3+}$ (Ln = La, Gd; RE = Eu, Tb and Ce) powder phosphors

U. Rambabu [a,*], N.R. Munirathnam [a], T.L. Prakash [a], S. Buddhudu [b]

[a] *Centre for Materials for Electronics Technology (C-MET), IDA Phase-II, HCL (Post), Cherlapally, Hyderabad 500051, India*
[b] *Department of Physics, Sri Venkateswara University, Tirupati 517502, India*

Received 31 December 2001; received in revised form 1 May 2002; accepted 10 May 2002

Abstract

This paper reports the emission spectra at room temperature and presents an optimum concentration for each of the dopants in $GdPO_4:Eu^{3+}$, $LaPO_4:Tb^{3+}$ and $LaPO_4:Ce^{3+}$ powder phosphors for the observation of bright reddish-orange, green and UV emission, respectively. FT-IR and a thermal analysis of these phosphor materials have been carried out. Scanning electron microscopic investigations were also conducted to understand surface morphological features (shape) and the grain size in the powder phosphor systems.

Keywords: Lanthanide phosphates; Eu^{3+}, Tb^{3+} and Ce^{3+} dopants; Optimum concentration

1. Introduction

Fluorescence spectra of rare earth activated materials have potential industrial applications, for example, in solid state lasers (YAG:Nd), in color TV monitors (Y_2O_2S:Eu) and in X-ray intensifying screens (LaOBr:Tb) [1,2]. Lanthanide orthophosphates ($LnPO_4$) crystallize in two polymorphic types, the monoclinic monazite type (for Ln = La to Gd) and the quadratic xenotime type (for Ln = Tb to Lu). The emission spectrum of Eu^{3+} in $LnPO_4$ was reported for the first time by Ropp [3] who compared the emission intensities of the rare earth phosphates and rare earth oxide phosphors. The highly efficient Tb^{3+}-doped monazite phase ($La_xTb_yCe_z$) PO_4 has been a green phosphor in fluorescent lamps [4–6]. Ropp who reported that Ce^{3+}-activated rare earth phosphates have lifetimes in the nanosecond range [7]. $YPO_4:Ce^{3+}$ displays two UV emission peaks [3,7]. Schwarz and coworkers [8–10] and Brabier et al. [11] have carried out the optical investigations of alkali rare earth phosphates of the type $M_3RE(PO_4)_2$ (M = Na, K, Rb; RE = La to Tb). Erdei et al. [12,13] prepared Ce^{3+}, Tb^{3+}:$LaPO_4$ green phosphors by a newly developed hydrolyzed colloidal reaction (HCR) technique at room temperature (<100 °C) and in atmospheric pressure by utilizing a subsequent calcining and reductive treatments, respectively. Brixner and Fluornoy have mentioned some of the properties of the $GdPO_4:Eu^{3+}$ phosphors and compared them with other hosts. Over the past few years, we have been actively involved in the preparation and characterization of a wide variety of rare earth doped powder phosphors for their use in color TV monitors, fluorescent lamps and X-ray intensifying screens [14–16]. Keeping in view the commercial applications of red, green and blue emitting phosphors, earlier we have prepared and characterized the Eu^{3+}, Tb^{3+} and Ce^{3+}-doped lanthanide oxychloride, $Na_6Ln(BO_3)_3$ (Ln = La and Gd), lanthanide oxyfluoride and oxybromide powder phosphors [17–21]. The purpose of present paper is to report the synthesis, optical properties and the optimization of dopant ion (Eu^{3+}, Tb^{3+} and Ce^{3+}) concentration in lanthanide based phosphors.

2. Experimental

Lanthanide phosphates can be synthesized through different reactions and/or in combinations as well. Here, we have adopted a precipitation technique, which involves a direct and clean reaction between the lanthanide oxides and phosphoric acid without any by-products other than the water [22]. For the synthesis of these phosphors, ultra pure gadolinium oxide (Gd_2O_3), lanthanum oxide (La_2O_3), yttrium oxide (Y_2O_3), europium oxide (Eu_2O_3), terbium oxide (Tb_4O_7), cerium oxide (CeO_2) and phosphoric acid (H_3PO_4)

* Corresponding author. Present address: Institute of Electro-Optical Engineering, National Chiao-Tung University, R. No. 518, MIRC Building, Hsinchu, Taiwan, ROC.
E-mail address: urambabu@yahoo.com (U. Rambabu).

0254-0584/02/$ – see front matter
PII: S0254-0584(02)00294-8

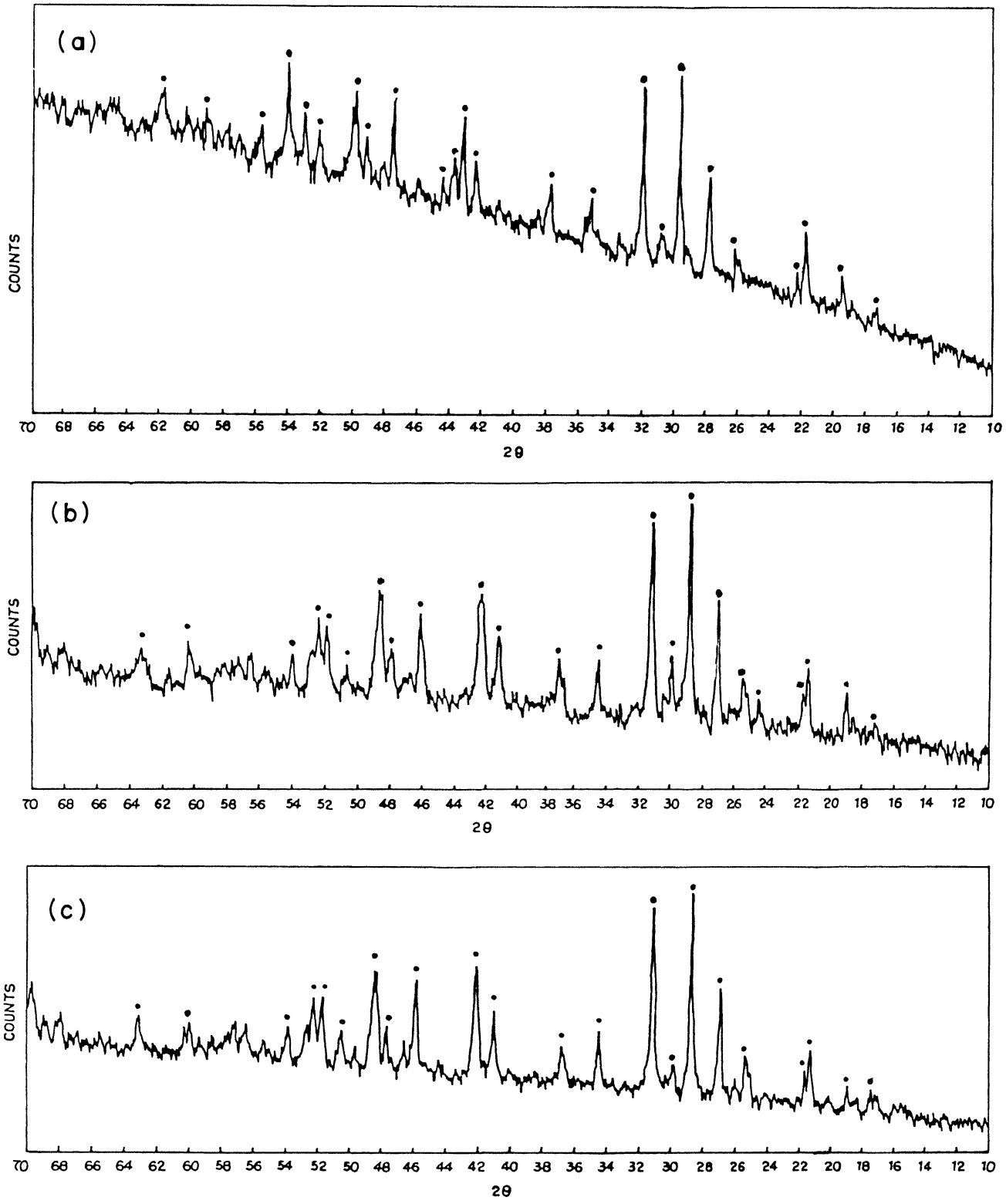

Fig. 1. XRD patterns of (a) $Gd_{0.95}PO_4:Eu_{0.05}^{3+}$, (b) $La_{0.95}PO_4:Tb_{0.05}^{3+}$ and (c) $La_{0.95}PO_4:Ce_{0.05}^{3+}$ powder phosphors.

were taken as the starting chemicals. Due to the hygroscopic nature of the lanthanide oxides, the starting oxides were calcined at 700 °C [23]. Initially, chemicals pertaining to following compositions were mixed thoroughly by using acetone as the mixing medium. For labeling purpose, the reddish-orange color emitting (Eu^{3+}) phosphors are abbreviated as RP, green color emitting (Tb^{3+}) phosphors as GP and UV emission (Ce^{3+}) phosphors as UVP with the phosphor sample numbers.

1. $Gd_{0.999}PO_4:Eu_{0.001}^{3+}$ (RP-1)
2. $Gd_{0.995}PO_4:Eu_{0.005}^{3+}$ (RP-2)
3. $Gd_{0.99}PO_4:Eu_{0.01}^{3+}$ (RP-3)
4. $Gd_{0.95}PO_4:Eu_{0.05}^{3+}$ (RP-4)
5. $Gd_{0.9}PO_4:Eu_{0.1}^{3+}$ (RP-5)

1. $La_{0.995}PO_4:Tb_{0.005}^{3+}$ (GP-1)
2. $La_{0.99}PO_4:Tb_{0.01}^{3+}$ (GP-2)
3. $La_{0.95}PO_4:Tb_{0.05}^{3+}$ (GP-3)
4. $La_{0.9}PO_4:Tb_{0.1}^{3+}$ (GP-4)
5. $La_{0.5}PO_4:Tb_{0.5}^{3+}$ (GP-5)

1. $La_{0.995}PO_4:Ce_{0.005}^{3+}$ (UVP-1)
2. $La_{0.99}PO_4:Ce_{0.01}^{3+}$ (UVP-2)
3. $La_{0.95}PO_4:Ce_{0.05}^{3+}$ (UVP-3)
4. $La_{0.9}PO_4:Ce_{0.1}^{3+}$ (UVP-4)
5. $La_{0.6}PO_4:Ce_{0.4}^{3+}$ (UVP-5)

The dried lanthanide oxide powders were slowly added to a 85% phosphoric acid. The reaction was vigorous and exothermic in nature. Large precipitates were immediately formed at the reaction site, and then broke into fine particles. The solution was extremely dense and stable and did not separate for a long period of time. The solution was later stirred for 30 min and then separated by centrifuging. Traces of excess H_3PO_4 were removed by washing the samples several times with a deionized water. The chemical reaction involved in the present synthesis is as follows:

$$(1-x)Ln_2O_3 + xRE_2O_3 + 2H_3PO_4 \rightarrow 2Ln_{1-x}RE_x + 3H_2O$$

(Ln = La and Gd; RE = Eu, Tb and Ce)

($0.001 \leq x \leq 0.5$)

The obtained white powders were collected into quartz boats and fired in a silica tube in the central zone of a high temperature furnace for 3 h at 950 °C in an inert (N_2) atmosphere. Soon after completion of the synthesis, the emission under an UV source is reddish-orange, green and ultraviolet for the Eu^{3+}, Tb^{3+} and Ce^{3+} phosphors, respectively. The purity of the synthesized phosphors $Gd_{0.95}PO_4:Eu_{0.05}^{3+}$, $La_{0.95}PO_4:Tb_{0.05}^{3+}$ and $La_{0.95}PO_4:Ce_{0.05}^{3+}$ was checked by X-ray diffractometry (XRD). A Philips PW 18140 X-ray diffractometer fitted with a PM 820 3A online recorder was used for this purpose. All diffractograms were recorded with Cu Kα ($\lambda = 0.1542$ nm) radiation (Fig. 1(a)–(c)) [22]. Both excitation and fluorescence spectra of these phosphors were recorded on a Hitachi 650 10S spectrofluorimeter using a 150 W xenon arc lamp as the excitation source at room temperature. The recorded excitation spectra are shown in Fig. 2(a)–(c), revealing the stronger lines of excitation, $\lambda_{exc} = 398$ nm (Eu^{3+}), $\lambda_{exc} = 370$ nm (Tb^{3+}), and $\lambda_{exc} = 258$ nm (Ce^{3+}). The fluorescence spectra are shown in the Figs. 3–5. The FT-IR absorption spectra of these samples were carried out on a Perkin-Elmer spectrometer (spectrum 2000) with KBr pellets in the wave-number range of 1400–370 cm^{-1} given in Fig. 6(a)–(c) [24]. The surface morphological features (shape and grain-size) of the phosphors $Gd_{0.95}PO_4:Eu_{0.05}^{3+}$, $La_{0.95}PO_4:Tb_{0.05}^{3+}$ and $La_{0.95}PO_4:Ce_{0.05}^{3+}$ were studied by using Leica stereoscan 440 scanning electron microscope (SEM). SEM photographs are furnished in Fig. 7(a)–(c). For SEM analysis, the samples were pre-coated with a thin layer of gold in a Polaran E5000 coating unit in order to prevent the charging of the specimen. For a comparative study, the electron beam parameters were kept constant while the analysis of the samples was being carried out. The SEM images of the samples with a 20 kV EHT and a 25 pA beam current were recorded by using a 35 mm camera attached on the high resolution recording unit. Thermogravimetric investigations (thermogravimetric analysis, TGA/differential thermal analysis, DTA) were carried out on the phosphor samples of $Gd_{0.95}PO_4:Eu_{0.05}^{3+}$, $La_{0.95}PO_4:Tb_{0.05}^{3+}$ and $La_{0.95}PO_4:Ce_{0.05}^{3+}$ by using Mettler Toledo TGA/SDTA 851^e. The samples were heated from 900 to 1300 °C in a dynamic inert (N_2) atmosphere and with the heating rate of 10 °C min^{-1}. TGA/DTA results are produced in Fig. 8(a1/b1), (a2/b2) and (a3/b3), respectively.

3. Results and discussion

3.1. Eu^{3+}:phosphors

The profiles of the fluorescence spectra of all Eu^{3+}:phosphors (Fig. 3) show the emission transitions [25]:

$^5D_0 \rightarrow {}^7F_4, {}^7F_3, {}^7F_2, {}^7F_1$ and $^7F_0$

The main emission peaks are located at 580–591 nm ($^5D_0 \rightarrow {}^7F_1$) and at 610–619 nm ($^5D_0 \rightarrow {}^7F_2$), respectively. The transition ($^5D_0 \rightarrow {}^7F_2$) splits into three components and similarly the other transition ($^5D_0 \rightarrow {}^7F_1$) (magnetic dipole in character) is split into two components in all the Eu^{3+}:phosphors. The presence of a sensitive forbidden transition ($^5D_0 \rightarrow {}^7F_0$) has been identified in all phosphors with a very weak intensity. The transition ($^5D_0 \rightarrow {}^7F_1$) displays more intensity than that of the transition ($^5D_0 \rightarrow {}^7F_2$) due to localized energy transfer. Usually, for non-centro symmetrical host-compounds including Eu^{3+}-doped lanthanide oxychloride, lanthanide-alkaline earth borates and lanthanide oxybromides, which we studied

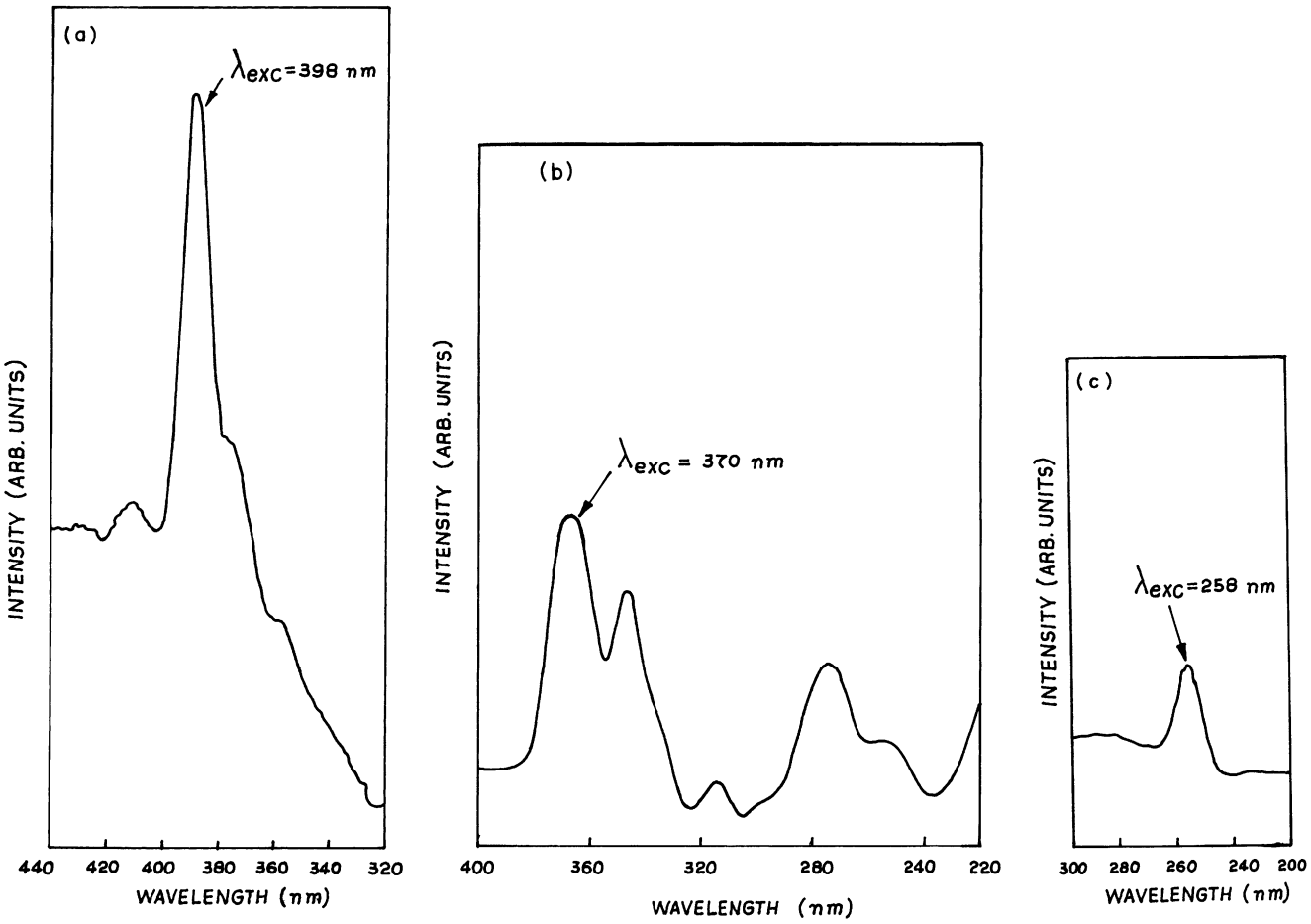

Fig. 2. Excitation spectra of (a) $Gd_{0.999}PO_4:Eu_{0.001}^{3+}$, (b) $La_{0.95}PO_4:Tb_{0.05}^{3+}$ and (c) $La_{0.95}PO_4:Ce_{0.05}^{3+}$ powder phosphors.

Table 1
Relative fluorescence intensity ratios (R) for the measured emission levels of $GdPO_4:Eu^{3+}$ powder phosphors

Phosphor	$(^5D_0 \rightarrow {}^7F_0)/(^5D_0 \rightarrow {}^7F_4)$	$(^5D_0 \rightarrow {}^7F_1)/(^5D_0 \rightarrow {}^7F_4)$	$(^5D_0 \rightarrow {}^7F_2)/(^5D_0 \rightarrow {}^7F_4)$	$(^5D_0 \rightarrow {}^7F_3)/(^5D_0 \rightarrow {}^7F_4)$	$(^5D_0 \rightarrow {}^7F_4)/(^5D_0 \rightarrow {}^7F_4)$
RP-1	–	1.464	1.071	0.803	1.000
		1.571	0.928		0.857
			0.964		1.000
RP-2	–	1.820	1.179	0.641	1.000
		2.038	0.858		0.743
			0.935		1.038
RP-3	–	1.980	1.200	0.530	1.000
		2.260	0.800		0.680
			0.920		1.050
RP-4	0.232	2.341	1.261	0.295	1.000
		2.785	0.693		0.505
			0.835		1.051
RP-5	0.333	1.993	1.178	0.392	1.000
		2.440	0.720		0.559
			0.845		1.000

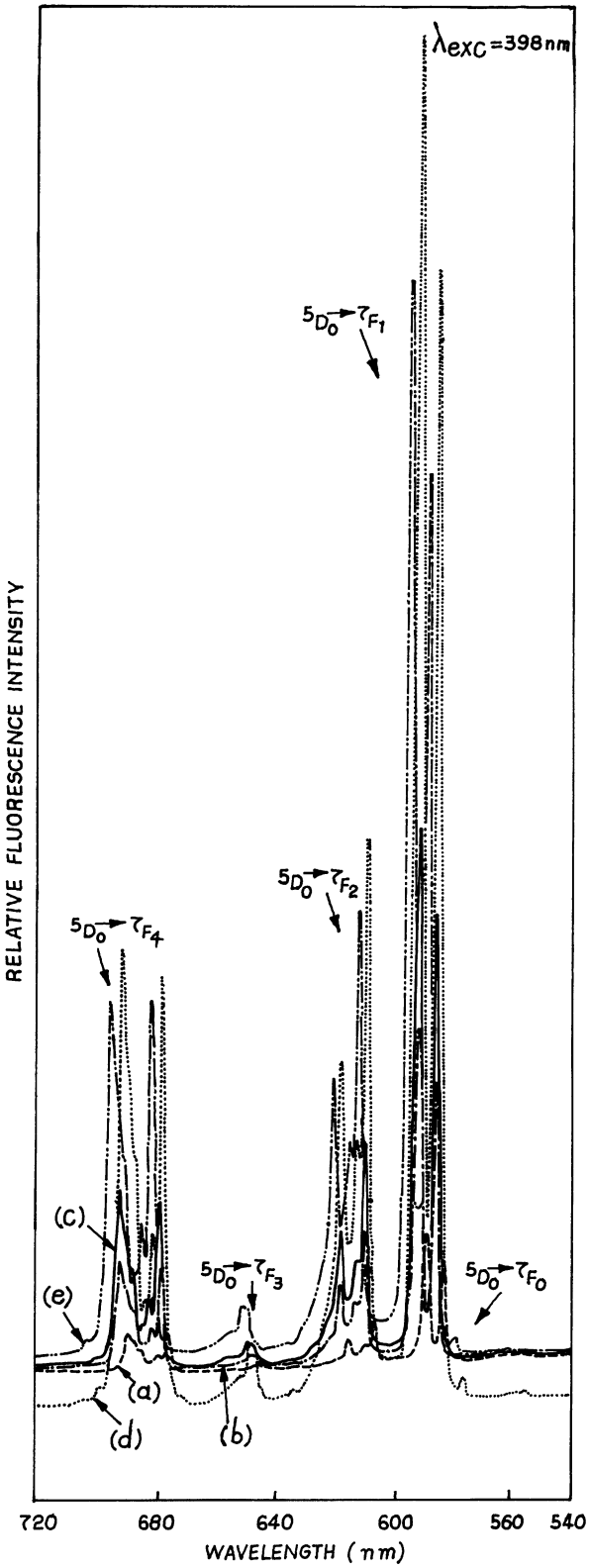

Fig. 3. Fluorescence spectra of (a) $Gd_{0.999}PO_4$:$Eu_{0.001}^{3+}$, (b) $Gd_{0.995}PO_4$:$Eu_{0.005}^{3+}$, (c) $Gd_{0.99}PO_4$:$Eu_{0.01}^{3+}$, (d) $Gd_{0.95}PO_4$:$Eu_{0.05}^{3+}$ and (e) $Gd_{0.9}PO_4$:$Eu_{0.1}^{3+}$ powder phosphors.

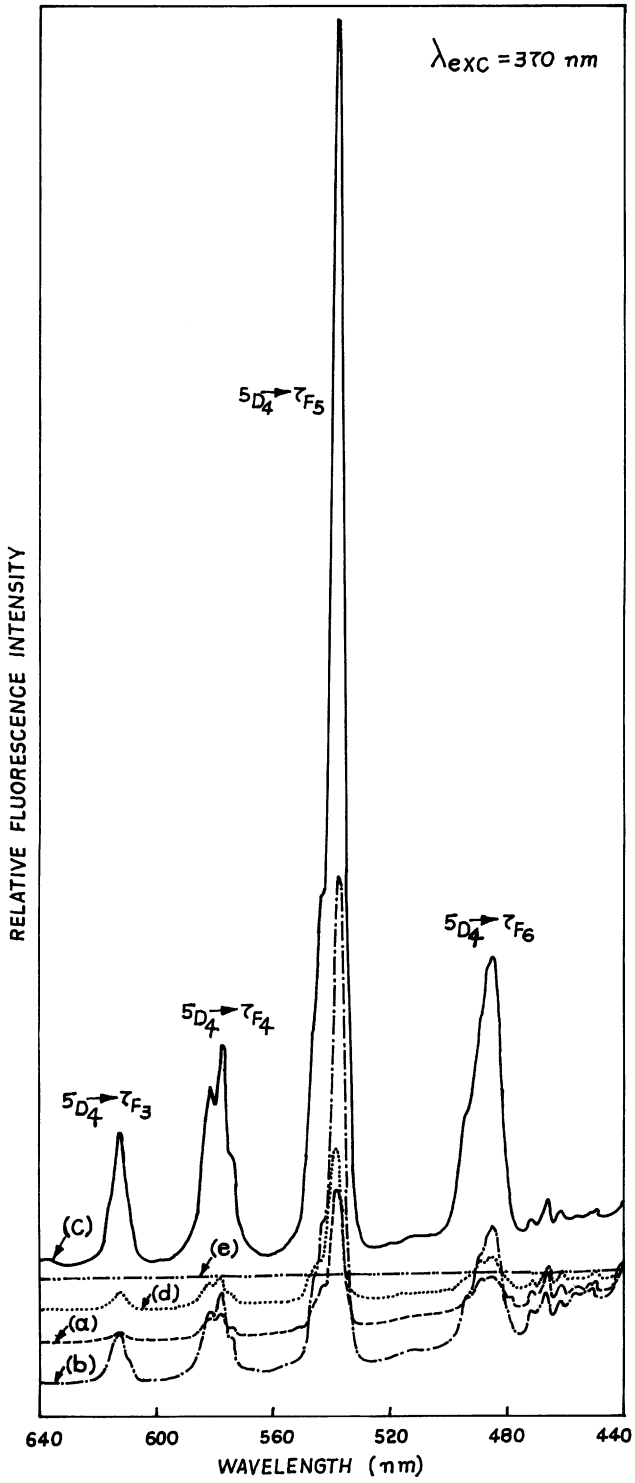

Fig. 4. Fluorescence spectra of (a) $La_{0.995}PO_4$:$Tb_{0.005}^{3+}$, (b) $La_{0.99}PO_4$:$Tb_{0.01}^{3+}$, (c) $La_{0.95}PO_4$:$Tb_{0.05}^{3+}$, (d) $La_{0.9}PO_4$:$Tb_{0.1}^{3+}$ and (e) $La_{0.5}PO_4$:$Tb_{0.5}^{3+}$ powder phosphors.

earlier, the ($^5D_0 \rightarrow {}^7F_2$) transition is the most intense one [17–20]. The emission transitions have assigned using the data from the literature [4]. The intensity of the emission transitions was found to increase with an increase in Eu concentration up to 5 mol. Additionally, the emission peak

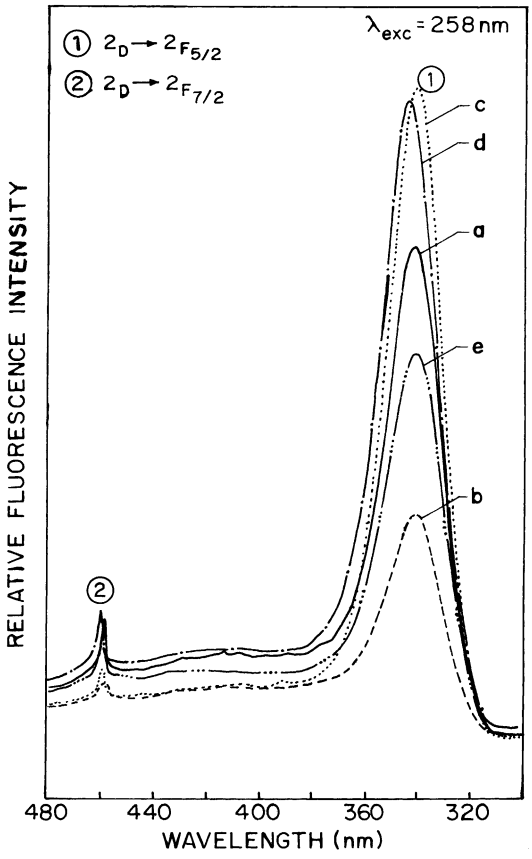

Fig. 5. Fluorescence spectra of (a) $La_{0.995}PO_4:Ce_{0.005}^{3+}$, (b) $La_{0.99}PO_4:Ce_{0.01}^{3+}$, (c) $La_{0.95}PO_4:Ce_{0.05}^{3+}$, (d) $La_{0.9}PO_4:Ce_{0.1}^{3+}$ and (e) $La_{0.6}PO_4:Ce_{0.4}^{3+}$ powder phosphors.

Table 2
The emission level peak positions (λ_p, nm) for the transition ($^5D_0 \rightarrow {}^7F_2$) and color coordinates ($\bar{X}$, $\bar{Y}$) of $GdPO_4:Eu^{3+}$ powder phosphors

Phosphor	λ_p (nm)	$\bar{X}$	$\bar{Y}$
RP-1	606 614	0.516	0.450
RP-2	608 616	0.621	0.377
RP-3	609 618	0.616	0.382
RP-4	610 619	0.625	0.373
RP-5	611 619	0.657	0.341

positions are found to be marginally shifted towards the higher wavelength side. The relative fluorescence intensity ratios (R), have been calculated and given in Table 1. The emission level peak positions (λ_p, nm) for the transition ($^5D_0 \rightarrow {}^7F_2$), is given in Table 2, which are noticed to significantly change with the chemical composition. Color coordinates ($\bar{X}$, $\bar{Y}$) are computed according to standard formulations made available by the Commission Internationale de 1'Eclairage (CIE), France, and based on the three primary colors red, green and blue (Table 2) [26]. The computed color coordinates ($\bar{X}$, $\bar{Y}$) are superimposed in the CIE chromaticity diagram to check the validity of the obtained results (Fig. 9). From Fig. 9, it is clear that the color coordinates of the synthesized powder phosphors are well fitted

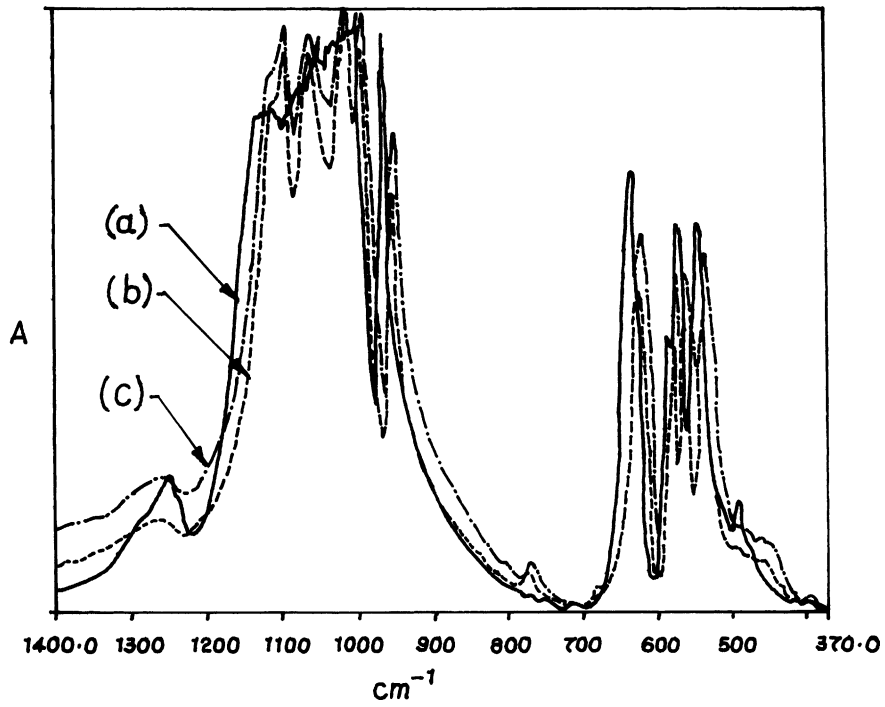

Fig. 6. FT-IR absorption spectra of (a) $Gd_{0.95}PO_4:Eu_{0.05}^{3+}$, (b) $La_{0.95}PO_4:Tb_{0.05}^{3+}$ and (c) $La_{0.95}PO_4:Ce_{0.05}^{3+}$ powder phosphors.

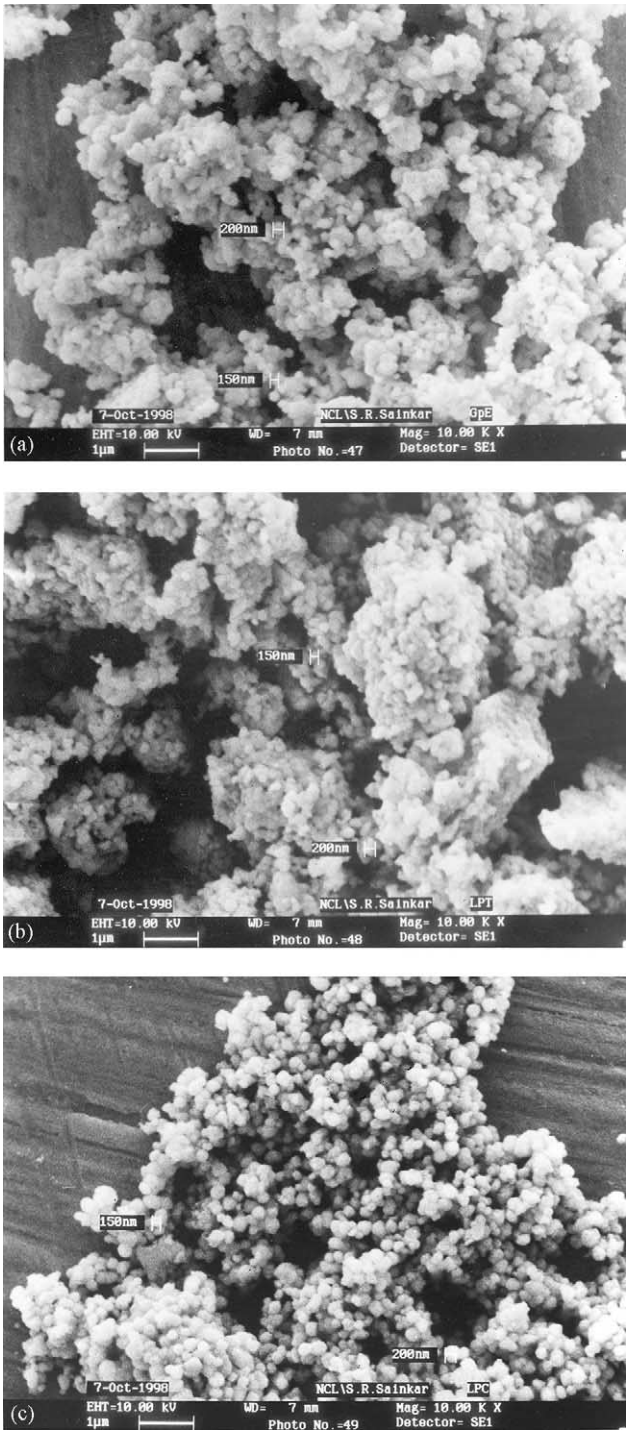

Fig. 7. SEM images of (a) $Gd_{0.95}PO_4:Eu_{0.05}^{3+}$, (b) $La_{0.95}PO_4:Tb_{0.05}^{3+}$ and (c) $La_{0.95}PO_4:Ce_{0.05}^{3+}$ powder phosphors.

in the reddish-orange region (indicated as a rectangular shaded portion). The recorded FT-IR absorption spectrum of $Gd_{0.95}PO_4:Eu_{0.05}^{3+}$ Fig. 6(a)) has been in agreement with the reported literature [24]. The ionic phosphate absorption is reported on the basis of the Raman work to absorb at 1080 and 980 cm^{-1} [27]. The fundamental frequencies allowed in the infrared appear at 500 cm^{-1}. In the pertinent FT-IR spectrum, two bunches of absorption bands have been observed in the wave-number region 1200–900 and 700–400 cm^{-1} which are attributed to M–OPO_3 (M = Gd and Eu) bonds [28]. Thermogravimetry of $Gd_{0.95}PO_4:Eu_{0.05}^{3+}$, indicates the total thermal stability with respect to chemical as well as crystalline phase transformation changes, in a covered temperature range. From the recorded SEM image of $Gd_{0.95}PO_4:Eu_{0.05}^{3+}$ (Fig. 7(a)), it is seen that, the particles are agglomerated and are having a spherical shape with a grain size in the range of 150–200 nm. Based on the recorded fluorescence spectral features and from the relative fluorescence intensity ratios (R), the optimum concentration of the dopant europium (Eu^{3+}) has been found to be 5 mol.

3.2. Tb^{3+}:phosphors

From the recorded fluorescence spectra of Tb^{3+}:phosphors (Fig. 4), the following four emission transitions have been observed [12,29–31]:

- $^5D_4 \rightarrow {}^7F_6$ (486–484 nm)
- $^5D_4 \rightarrow {}^7F_5$ (539–537 nm)
- $^5D_4 \rightarrow {}^7F_4$ (578–577 nm)
- $^5D_4 \rightarrow {}^7F_3$ (614–612 nm)

Among these, the emission transition $^5D_4 \rightarrow {}^7F_5$ is responsible for green color observation as a single peak, and it has been taken as a reference for the comparison of the fluorescence spectral peaks of the Tb^{3+}:phosphors studied. From the spectral features, it has been noticed that, the intensity of the emission peaks increases with an increase in terbium concentration up to 5 mol beyond which the fluorescence quenching has been observed. Besides this, positions of the emission peaks have been observed to be varying slightly depending upon the host matrix. Therefore, the Tb^{3+} concentration of 5 mol has been found to be an optimum dopant ion concentration. The emission level peak positions (λ_p, nm) of the transition $^5D_4 \rightarrow {}^7F_5$ are given in Table 3. As in Eu^{3+}:phosphors, Tb^{3+}:phosphors were also characterized by computing the color coordinates ($\bar{X}$, $\bar{Y}$) (Table 3) and relative fluorescence intensity ratios (R) (Table 4). The obtained color coordinates ($\bar{X}$, $\bar{Y}$) are superimposed on the CIE chromaticity diagram (Fig. 9) to assess the color richness of the synthesized powder phosphors [19]. From Fig. 9, it is clear that the

Table 3
Emission level peak positions (λ_p, nm) for the transitions $^5D_4 \rightarrow {}^7F_5$ and color coordinates ($\bar{X}$, $\bar{Y}$) of $LaPO_4:Tb^{3+}$ powder phosphors

Phosphor	λ_p (nm)	$\bar{X}$	$\bar{Y}$
GP-1	538	0.245	0.409
GP-2	537	0.225	0.436
GP-3	538	0.271	0.480
GP-4	539	0.262	0.427
GP-5	–	0.283	0.424

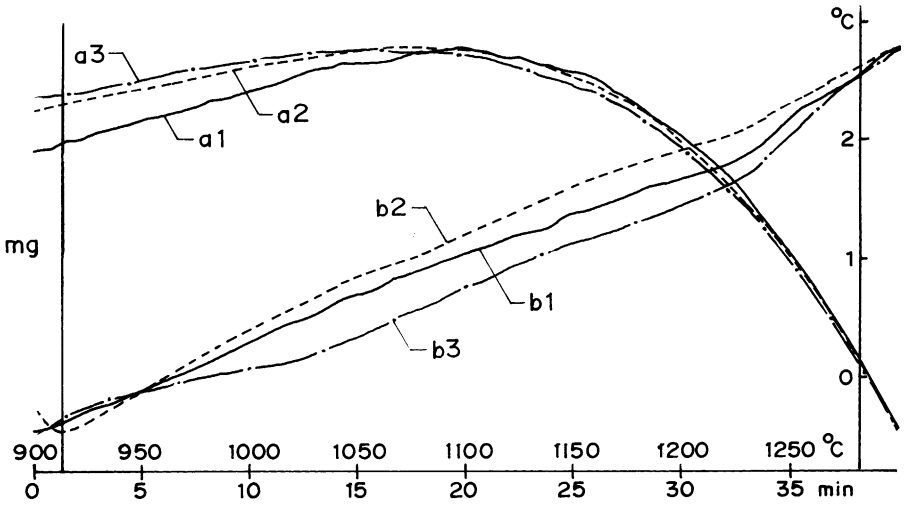

Fig. 8. TGA/DTA curves of (a1/b1) $Gd_{0.95}PO_4:Eu_{0.05}^{3+}$, (a2/b2) $La_{0.95}PO_4:Tb_{0.05}^{3+}$ and (a3/b3) $La_{0.95}PO_4:Ce_{0.05}^{3+}$ powder phosphors.

obtained color coordinates ($\bar{X}$, $\bar{Y}$) are fitted appropriately in the green region (indicated by a marked portion). TGA of $La_{0.95}PO_4:Tb_{0.05}^{3+}$ indicates the total 0.311% weight loss out of 54.6 mg. No appreciable weight loss in TGA (Fig. 8(a2)) and absence of any noticeable peak in DTA (Fig. 8(b2)) mode indicates thermal stability with respect to chemical as well as crystalline phase transformation changes, in a covered temperature range. As discussed in FT-IR spectrum of $Gd_{0.95}PO_4:Eu_{0.05}^{3+}$ phosphor, in $La_{0.95}PO_4:Tb_{0.05}^{3+}$ (Fig. 6(b)), also we have observed two bunches of absorption frequencies attributable to complex M–OPO_3 (M = La, Tb) bonds in the wave-number range 1200–900 and 700–400 cm^{-1}, with noticeable little shift in the absorption frequencies [24,28]. From the recorded SEM image of the samples $La_{0.95}PO_4:Tb_{0.05}^{3+}$ (Fig. 7(b)), it is seen that the individual spherical particles are agglomerated. The grain size is observed to be in the range of 150–200 nm. Based on the computed color coordinates and relative fluorescence intensity ratios (R), the optimum

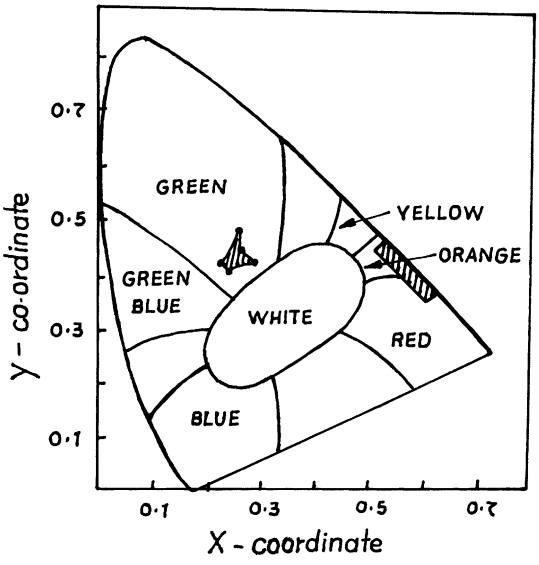

Fig. 9. CIE chromaticity diagram.

Table 4
Relative fluorescence intensity ratios (R) of $LaPO_4:Tb^{3+}$ powder phosphors

Phosphor	$(^5D_4 \rightarrow {}^7F_3)/(^5D_4 \rightarrow {}^7F_6)$	$(^5D_4 \rightarrow {}^7F_4)/(^5D_4 \rightarrow {}^7F_6)$	$(^5D_4 \rightarrow {}^7F)_5/(^5D_4 \rightarrow {}^7F_6)$	$(^5D_4 \rightarrow {}^7F_6)/(^5D_4 \rightarrow {}^7F_6)$
GP-1	0.583	0.708 0.750 0.666	1.583	1.000
GP-2	0.437	0.562 0.656 0.437	2.875	1.000
GP-3	0.620	0.721 0.810 0.569	3.025	1.000
GP-4	0.814	0.851 0.888 0.777	1.740	1.000
GP-5	–	–	–	–

Table 5
The relative fluorescence intensity ratios (R), emission level peak positions (λ_p, nm) and half width at full maxima ($\Delta\lambda_p$, nm) for the transition $^2D \rightarrow {}^2F_{5/2}$ of $LaPO_4:Ce^{3+}$ phosphors

Phosphor	$(^2D \rightarrow {}^2F_{5/2})/(^2D \rightarrow {}^2F_{7/2})$ (R)	λ_p	$\Delta\lambda_p$
UVP-1	10.22	342	26.10
UVP-2	8.20	341	26.10
UVP-3	24.4	342	24.10
UVP-4	11.9	341	26.10
UVP-5	9.0	341	28.10

concentration of the dopant ion (Tb^{3+}) has been found to be 5 mol.

3.3. Ce^{3+}:phosphors

The trivalent Ce^{3+}-ions have an electronic structure containing one 4f-electron and as an activator, they generally result in phosphors having broad band UV emission. In the rare earth phosphates, the emission bands of Ce^{3+} are not like those found in other materials [3]. From the measured fluorescence spectra (Fig. 5) of Ce^{3+}:phosphors, two bands corresponding to the following electronic transitions are identified [7,32,33]:

- ^2D (5d) $\rightarrow {}^2F_{5/2}$ (4f) (342–341 nm)
- ^2D (5d) $\rightarrow {}^2F_{7/2}$ (4f) (460–458 nm)

The emission transition $^2D \rightarrow {}^2F_{5/2}$ appears more intense and broader in all Ce^{3+}:phosphors. The fluorescence intensity increase with an increase in Ce concentration up to 5 mol, beyond which, the fluorescence intensity tends to quench. It is also noticed that the peak positions of the emission bands have also changed significantly. Since, these phosphors are emitting in the UV region, we could not compute the color coordinates ($\bar{X}$, $\bar{Y}$), however the emission level peak positions (λ_p, nm) and their effective half width at full maxima ($\Delta\lambda_p$, nm) are given in Table 5, which significantly change with the chemical composition. The synthesized powder phosphors are also characterized by calculating the relative fluorescence intensity ratios (R) (Table 5). TGA of $La_{0.95}PO_4:Ce_{0.05}{}^{3+}$ indicates the total 0.344% weight loss out of 66.73 mg. No appreciable weight loss in TGA (Fig. 8(a3)) and the absence of any noticeable peak in DTA (Fig. 8(b3)) mode indicates thermal stability with respect to chemical as well as crystalline phase transformation changes, in a covered temperature range. As has been discussed earlier, $La_{0.95}PO_4:Ce_{0.05}{}^{3+}$ also gives same absorption peaks except a few cm^{-1} shift in the frequencies (Fig. 6(c)) [28]. From the SEM image of $La_{0.95}PO_4:Ce_{0.05}{}^{3+}$ (Fig. 7(c)), it has been noticed that the particles are having spherical shape which tend to agglomerate and size in the range of 150–200 nm. Based on the relative fluorescence intensity ratios (R), the concentration of the dopant ion Ce^{3+} has been optimized to be 5 mol.

4. Conclusions

We have synthesized rich color emitting Eu^{3+}, Tb^{3+}, and Ce^{3+}-doped powder phosphors by employing a precipitation technique. The phase purity has been verified by XRD and a FT-IR spectral analysis. Based on the color coordinates ($\bar{X}$, $\bar{Y}$) and relative fluorescence intensity ratios (R), the optimum concentration of each of the dopant ions (Eu^{3+}, Tb^{3+} and Ce^{3+}) has been identified to be 5 mol. From the scanning electron microscopic studies, it has been noticed that the particles are spherical in shape with size varying from 150 to 200 nm, and they tend to agglomerate. From the thermal analysis studies, it has been found that these phosphor materials are quite stable. A systematic studies could therefore result in the formulation of $Gd_{0.95}PO_4:Eu_{0.05}{}^{3+}$, $La_{0.95}PO_4:Tb_{0.05}{}^{3+}$ and $La_{0.95}PO_4:Ce_{0.05}{}^{3+}$ phosphors as the three materials in order to observe brighter reddish-orange, green and UV emission from certain electronic display systems.

Acknowledgements

One of the authors URB would like to express grateful thanks to Dr. B.K. Das, Executive Director, C-MET, Pune for his active support towards this work.

References

[1] A.P.D. Silva, V.A. Fassel, Anal. Chem. 45 (3) (1973) 542.
[2] L.H. Brixner, Mater. Chem. Phys. 16 (1987) 253.
[3] R.C. Ropp, J. Electrochem. Soc. 115 (1968) 841.
[4] J.D. Ghys, R. Mauricot, M.D. Faucher, J. Luminesc. 69 (1996) 203.
[5] R.C.L. Mooney, Acta. Cryst. 3 (1950) 338.
[6] W.A. McAllister, J. Electrochem. Soc. 115 (5) (1968) 535.
[7] R.C. Ropp, J. Electrochem. Soc. 115 (1968) 531.
[8] L. Schwarz, B. Finke, M. Kloss, A. Rohmann, U. Sasum, D. Haberland, J. Luminesc. 72–74 (1997) 257.
[9] M. Kloss, B. Finke, L. Schwarz, D. Haberland, J. Luminesc. 72–74 (1997) 684.
[10] B. Finke, L. Schwarz, P. Gurtler, M. Krass, M. Joppien, J. Becker, J. Luminesc. 60–61 (1994) 975.
[11] J. Brabier, J.E. Greedan, T. Asaro, G.J. McCarthy, Eur. J. Solid State Inorg. Chem. 27 (1990) 855.
[12] S. Erdei, F.W. Ainger, D. Ravichandran, W.B. White, L.E. Cross, Mater. Lett. 30 (1997) 389.
[13] S. Erdei, L. Kovacs, M. Martini, F. Meinardi, F.W. Ainger, W.B. White, J. Luminesc. 68 (1996) 27.
[14] U. Rambabu, K. Annapurna, T. Balaji, S. Buddhudu, Mater. Lett. 23 (1995) 143.
[15] U. Rambabu, K. Annapurna, T. Balaji, J.V.S. Narayana, S. Buddhudu, Spectrochim. Acta. A52 (1996) 367.
[16] U. Rambabu, T. Balaji, K. Annapurna, S. Buddhudu, Mater. Chem. Phys. 43 (1996) 195.
[17] U. Rambabu, T. Balaji, S. Buddhudu, Mater. Res. Bull. 30 (7) (1995) 891.
[18] U. Rambabu, K. Annapurna, T. Balaji, J.V.S. Narayana, K.R. Reddy, S. Buddhudu, Spectrosc. Lett. 29 (5) (1996) 833.
[19] U. Rambabu, P.K. Khanna, I.C. Rao, S. Buddhudu, Mater. Lett. 34 (1998) 269.

[20] C. Chateau, J. Holsa, J. Chem. Soc., Dalton Trans. 1575 (1990).
[21] U. Rambabu, T. Balaji, S. Buddhudu, B. Electrochem. 14 (11) (1998) 351.
[22] P. Chen, T. Ilmah, J. Mater. Sci. 32 (1997) 3863.
[23] R. Ray, H.A. McKinsty, Acta Crystallogr. 6 (1953) 365.
[24] U. Sasum, M. Kloss, A. Rohmann, L. Schwarz, D. Haberland, J. Luminesc. 72–74 (1997) 255.
[25] A. Bril, W.L. Wanmaker, B. Electrochem. Soc. 111 (12) (1964) 1363.
[26] R. Jagannathan, S.P. Manoharan, R.P. Rao, R.L. Narayana, J. Electrochem. 4 (6) (1988) 597.
[27] Herzberg, Infrared and Raman Spectra of Polyatomic Molecules, Van Nostrand, Princeton, NJ, 1945, 162 pp.
[28] A. Hezel, S.D. Ross, Spectrochim. Acta. 22 (1966) 1949.
[29] N. El Jouhari, C. Parent, G. Le Flem, J. Solid State Chem. 123 (1996) 398.
[30] S.L. Issler, C.C. Torardi, J. Alloys Compd. 229 (1995) 54.
[31] Y.-J. Wang, W.- Zhao, M.-Z. Su, J. Luminesc. 40–41 (1988) 177.
[32] T. Welker, C.R. Ronda, K.J.B.M. Niewesteeg, J. Electrochem. Soc. 138 (2) (1991) 602.
[33] T. Balaji, S. Buddhudu, Mater. Chem. Phys. 34 (1993) 310.